

Concordance between the Dynamics of Satellite Galaxies in the 2dFGRS and Λ CDM

Tereasa G. Brainerd

*Institute for Astrophysical Research, Boston University, 725 Commonwealth Ave., Boston,
MA 02215*

ABSTRACT

We compute the velocity dispersion profile, $\sigma_v(r_p)$, for the satellites of host galaxies in the Two Degree Field Galaxy Redshift Survey (2dFGRS) and in the Λ CDM GIF simulation. The host–satellite selection algorithm yields 1345 host galaxies in the 2dFGRS with luminosities in the range $0.5 L_{b_J}^* \leq L \leq 5.5 L_{b_J}^*$, for which a total of 2475 satellite galaxies is found. The magnitudes of the galaxies in the GIF simulation are converted to the b_J band pass, and hosts and satellites are selected in the same manner as in the 2dFGRS. On average, ~ 1200 hosts and ~ 4100 satellites are found in the GIF simulation, where the precise number depends upon the angle from which the simulation is viewed. Overall, there is excellent agreement between $\sigma_v(r_p)$ for the satellites in the 2dFGRS and the GIF simulation. On large scales, the velocity dispersion profiles for the complete samples decrease with projected radius, in good agreement with the expectations of a CDM universe. Further, there is a marked dependence of the velocity dispersion profile on both the host spectral type and the host luminosity. In particular, $\sigma_v(r_p)$ has a substantially higher amplitude and steeper slope for satellites of early–type hosts than it does for satellites of late–type hosts. In addition, both the amplitude and slope of $\sigma_v(r_p)$ increase with host luminosity. The velocity dispersion of satellites located within small projected radii from the host ($r_p \leq 120$ kpc) is only marginally consistent with the local B–band Tully–Fisher relation ($\sigma_v \propto L^{0.3}$) and is fitted best by a relationship of the form $\sigma_v \propto L^{0.45 \pm 0.10}$.

Subject headings: dark matter — galaxies: fundamental parameters – galaxies: halos — galaxies: kinematics and dynamics – surveys

1. Introduction

Although it is generally accepted that large, bright galaxies reside within massive halos of dark matter, the total mass, the radial dependence of the density profile and the physical extent of the halos remain poorly-constrained. A good amount of progress has been made, however, by the most recent investigations of weak galaxy–galaxy lensing (e.g., Fisher et al. 2000; Wilson et al. 2001; McKay et al. 2001; Smith et al. 2001; Guzik & Seljak 2002; Hoekstra et al. 2003; Kleinheinrich et al. 2003, 2004; Hoekstra, Yee & Gladders 2004) and this method certainly holds great promise for placing strong constraints on the nature of dark matter halos as a function of cosmic time. Ideally of course one would hope to determine the differences between the physical characteristics of the halos surrounding galaxies of differing Hubble type and differing luminosity, and weak lensing has begun to provide some interesting results regarding these characteristics. In particular, all studies of galaxy–galaxy lensing as a function of the lens Hubble type conclude that the velocity dispersion of the halos of early-type L^* galaxies and/or the mass-to-light ratios of early-type L^* galaxies exceed those of late-type L^* galaxies (e.g., Griffiths et al. 1996; McKay et al. 2001; Guzik & Seljak 2002; Kleinheinrich et al. 2003, 2004).

Although it is abundantly clear that galaxy–galaxy lensing is a very good tool for probing the halos of galaxies at large physical radii ($r \gtrsim 100h^{-1}$ kpc), the use of this technique to constrain dark matter halos as a function of galaxy morphology or galaxy luminosity is complicated by the fact that galaxy–galaxy lensing is inherently a multiple-deflection problem. This was first pointed out by Brainerd, Blandford & Smail (1996), hereafter BBS, in the context of their analysis of the first statistically-significant (4σ) detection of galaxy–galaxy lensing. In particular, BBS found that more than 50% of their source galaxies (apparent magnitudes of $23 < r < 24$) should have been lensed at a comparable and significant level by **two or more foreground galaxies** (apparent magnitudes of $20 < r < 23$). That is, for a given source galaxy, it was clear from the BBS data that the closest lens on the sky to any given source was not necessarily the only lens, and neither was it necessarily the strongest lens. (See, e.g., §3.6 of BBS.) Further work by Brainerd (2003, 2004) in an analysis of multiple weak deflections by the galaxies in the northern Hubble Deep Field has shown that the probability of multiple deflections of magnitude $\gamma = 0.005$ (a “significant” shear in the context of galaxy–galaxy lensing) exceeds 50% for source galaxies with $z_s \gtrsim 1$ when the median lens redshift is $z_l \sim 0.6$. Compared to the case in which only single deflections by the closest lens galaxy are included in the calculation, multiple weak deflections in galaxy–galaxy lensing result in a substantially higher net tangential shear about the lens centers and significantly correlated image ellipticities of the foreground and background galaxies on angular scales $\theta \lesssim 60''$. (See also Guzik & Seljak 2002 for a discussion of the contribution of group- and cluster-sized mass distributions to observations of galaxy–galaxy lensing at

lower redshifts.)

As a result of multiple weak deflections, then, computing the net weak lensing shear due to a particular population of lens galaxies (i.e., early-type vs. late-type; high-luminosity vs. low-luminosity) is not simple. That is, one cannot merely compute the tangential shear of source galaxies relative to, say, lens galaxies with late-type morphology and be certain that the shear is caused solely by single deflections due to lenses with late-type morphology. This is especially true in deep data sets (e.g., those for which the median lens redshift is $\gtrsim 0.5$). Instead, it is important to analyze and model the weak lensing signal in such a way that it accounts for the fact that multiple deflections are likely to have occurred in the data. That is not to say that weak lensing cannot provide reasonable constraints on the physical differences between halos surrounding galaxies of differing morphology or luminosity; rather, one simply has to be careful in how one arrives at those constraints.

This in mind, it is certainly worthwhile to consider the use of complementary methods to constrain the nature of dark matter halos, and one such method is, of course, the dynamics of satellite galaxies. Pioneering work by Zaritsky & White (1994) and Zaritsky et al. (1997) led to the conclusion that the halos of isolated spiral galaxies extend well beyond the optical radii and are extremely massive: $M(r \lesssim 150h^{-1} \text{ kpc}) \sim 1 - 2 \times 10^{12}h^{-1} M_{\odot}$. Despite these conscientious analyses, however, a certain skepticism regarding the usefulness of this technique remained owing to several important facts. First, the orbital timescales of the satellites is large (of order 5 to 20 Gyr at sufficiently large radii) and, therefore, virialization is by no means guaranteed. Second, there is no unique host/satellite selection algorithm which will insure the absence of “interlopers” from the data (i.e., galaxies which are falsely selected as satellites). Finally, the sample sizes in mid-1990’s were quite small (of order 70 hosts and 100 satellites), so the results were based on rather small number statistics.

In the past couple of years, however, the prospects for using the dynamics of satellite galaxies to study the dark matter halos of host galaxies has improved significantly. The advent of large redshift surveys such as the Sloan Digital Sky Survey (SDSS, York et al. 2000) and the Two Degree Field Galaxy Redshift Survey (2dFGRS; Colless et al. 2001, 2003) has increased the available samples of potential hosts and satellites by more than an order of magnitude. In addition, McKay et al. (2002) and Prada et al. (2003) have used data from both the SDSS and numerical simulations to show that the effects of interloper galaxies on the inferred velocity dispersion of satellite galaxies can be corrected straightforwardly by fitting a Gaussian plus a constant offset to the distribution of velocity differences, $|dv|$, between the hosts and satellites (see, e.g., Figs. 5 and 6 of Prada et al. 2003). Further, Prada et al. (2003) investigated a number of different algorithms for selecting hosts and satellites in the SDSS data, including the algorithm used by McKay et al. (2002), and found that the

results of their dynamical analyses were quite insensitive to the details of the host–satellite selection algorithm.

Simulations of galaxy redshift surveys by van den Bosch et al. (2004) seem to show that the fraction of interloper galaxies is substantially higher for host–satellite pairs with small values of $|dv|$ than it is for host–satellite pairs with large values of $|dv|$, an effect not taken into account by the recent investigations of satellite dynamics in large surveys. However, van den Bosch et al. (2004) also note that the inferred value of the velocity dispersion is very insensitive to the fraction of interloper galaxies and, hence, recently published values of σ_v based on a simple Gaussian–plus–offset fit are unlikely to be substantially in error.

In their analysis of the dynamics of satellite galaxies in the SDSS, McKay et al. (2002) found that the velocity dispersion of the satellites was independent of projected radius on the sky; i.e., their results were consistent with isothermal halos. However, a subsequent analysis of a larger subset of the SDSS data by Prada et al. (2003) showed that when the contamination of the velocity dispersion due to interlopers was expressly calculated as a function of projected radius (i.e., the fraction of interlopers increases with r_p), the velocity dispersion for the satellites surrounding the SDSS galaxies decreases with projected radius. This is in good agreement with the expectations for Navarro, Frenk & White (NFW) halos (e.g., Navarro, Frenk & White 1997, 1996, 1995), which are thought to be the most likely halo mass distribution in the context of hierarchical structure formation.

Brainerd & Specian (2003) used the 100K data release of the 2dFGRS to investigate the dynamics of satellite galaxies and, like Prada et al. (2003), Brainerd & Specian (2003) allowed for the fact that the interloper fraction was a strongly increasing function of projected radius. Unlike Prada et al. (2003), however, they found that the velocity dispersion of the satellites in the 2dFGRS was independent of projected radius and, therefore, that the halos of the 2dFGRS hosts were consistent with isothermal halos, not NFW halos. However, due to the relatively larger velocity errors in the 2dFGRS ($\sigma_{cz} \sim 85 \text{ km sec}^{-1}$ in the 2dFGRS vs. $\sigma_{cz} \sim 20 \text{ km sec}^{-1}$ in the SDSS) as well as the smaller sample size (~ 800 hosts and 1550 satellites in the 100K 2dFGRS data vs. ~ 1100 hosts and 2700 satellites in the SDSS), it is entirely possible that the apparent disagreement over the radial dependence of the velocity dispersion is due solely to the larger error bars in the Brainerd & Specian (2003) analysis.

Even more recently, Conroy et al. (2004) investigated the velocity dispersion profile yielded by 75 satellites surrounding 61 host galaxies in the DEEP2 redshift survey. Conroy et al. (2004) find that the velocity dispersion profile of an NFW halo with virial mass $M_{200} = 5.5 \times 10^{12} h^{-1} M_\odot$ is consistent with their measurements of $\sigma_v(r_p)$. However, a flat velocity dispersion profile (i.e., a singular isothermal sphere halo) is also formally consistent with their data and error bars.

In this paper we continue the efforts of Brainerd & Specian (2003) and investigate the dynamics of satellites in the final data release of the 2dFGRS. We compute the radial dependence of the satellite velocity dispersion as a function of both the host spectral type and the host luminosity. In addition, we compare the results from the 2dFGRS galaxies to those obtained by analyzing the dynamics of satellite galaxies in the present–epoch galaxy catalogs of the flat, Λ –dominated GIF simulation (Kauffmann et al. 1999). This is a publicly–available simulation which includes semi–analytic galaxy formation in a cold dark matter (CDM) universe. The paper is organized as follows. The selection of hosts and satellites is discussed in §2. The computation of the satellite velocity dispersion, $\sigma_v(r_p)$, and the correction of $\sigma_v(r_p)$ for velocity errors is discussed in §3. Results are shown in §4, and a discussion of our results, including a comparison with previous work, is presented in §5.

2. Selection of Hosts and Satellites

2.1. 2dFGRS Galaxies

The 2dFGRS is a spectroscopic survey in which the target objects were selected in the b_J band from the Automated Plate Measuring (APM) galaxy survey (Maddox et al. 1990a, 1990b) and extensions to the original survey. The final data release occurred on June 30, 2003 (Colless et al. 2003) and includes redshifts of 221,414 galaxies brighter than $b_J = 19.45$ over ~ 1500 square degrees. All data, including spectroscopic and photometric catalogs, are publicly–available from the 2dFGRS website (<http://msowww.anu.edu/au/2dFGRS>), as well as DVDs that can be ordered from the 2dFGRS team. The photometric transformation from the SDSS band passes to b_J is

$$b_J = g' + 0.155 + 0.152(g' - r') \quad (1)$$

(Norberg et al. 2002) and the absolute magnitude of an $L_{b_J}^*$ galaxy is given by

$$M_{b_J}^* = -19.58 \pm 0.05 + 5 \log_{10} h, \quad \eta < -1.4 \quad (2a)$$

$$M_{b_J}^* = -19.53 \pm 0.03 + 5 \log_{10} h, \quad -1.4 \leq \eta < 1.1 \quad (2b)$$

$$M_{b_J}^* = -19.17 \pm 0.04 + 5 \log_{10} h, \quad 1.1 \leq \eta < 3.5 \quad (2c)$$

$$M_{b_J}^* = -19.15 \pm 0.05 + 5 \log_{10} h, \quad \eta \geq 3.5 \quad (2d)$$

where η is the spectral type of the galaxy (Madgwick et al. 2002). Galaxies with large negative values of η have spectra that are dominated by absorption features, and those with large positive values of η have spectra that are dominated by emission lines. Here, and throughout this paper, we adopt the following values of the cosmological parameters: $\Omega_0 = 0.3$, $\Lambda_0 = 0.7$, $H_0 = 70 \text{ km sec}^{-1} \text{ Mpc}^{-1}$.

We select a preliminary set of hosts and satellites from the 2dFGRS using criteria identical to those of McKay et al. (2002), Brainerd & Specian (2003), and Prada et al. (2003):

1. Host galaxies must be “isolated”. They must be at least twice as luminous as any other galaxy that falls within a projected radius of $2 h^{-1} \text{ Mpc}$ and a velocity difference of $|dv| \leq 1000 \text{ km sec}^{-1}$.
2. Potential satellites must be at least 4 times fainter than their host, must fall within a projected radius of $500h^{-1} \text{ kpc}$, and the velocity difference between the host and the satellite must be $|dv| \leq 1000 \text{ km sec}^{-1}$.

In addition to the above criteria, we impose an additional restriction that the sum total of the luminosities of the satellites must be less than the luminosity of the host. This was also done by McKay et al. (2002), Prada et al. (2003), and Brainerd & Specian (2003) in order to eliminate a handful of hosts for which the number of satellites is extremely large and, hence, objects which are more likely to be in a cluster environment rather than being truly isolated. Further, we eliminate a small number of hosts for which the eyeball morphology provided by the 2dFGRS team falls into the interaction/merger category, on the grounds that these are dynamically young systems which are unlikely to be virialized. Also, since we will ultimately be interested in investigating satellite dynamics as a function of host spectral type, we eliminate a small number of hosts for which no spectral classification parameter, η , was provided by the 2dFGRS team. Finally, we restrict our analysis to hosts with luminosities in the range $0.5 L_{b,j}^* \leq L \leq 5.5 L_{b,j}^*$ since there are relatively few hosts with $L < 0.5 L_{b,j}^*$ and the distribution of the host–satellite velocity differences for hosts with $L \gg 5 L_{b,j}^*$ is poorly–fitted by the technique which we adopt (see below). This leaves us with a final sample that consists of 1345 hosts and 2475 satellites. The median redshift of the hosts is $z = 0.08$.

The normalized probability distribution of the 2dFGRS host luminosities is shown in the left panel of Fig. 1, and the normalized probability distribution of the number of satellites per host is shown in the left panel of Fig. 2. The 2dFGRS sample is clearly dominated by systems containing 1 or 2 satellites per host, with only $\sim 20\%$ of hosts having 3 or more satellites.

2.2. GIF Galaxies

In order to compare our results for the 2dFGRS hosts to that expected for large, bright galaxies in a flat, Λ -dominated CDM universe, we have used one of the publicly-available GIF simulations to select samples of theoretical hosts and satellites. The entire suite of GIF simulations consists of N-body, adaptive P³M simulations of various CDM universes, coupled with a semi-analytic prescription for galaxy formation (see, e.g., Kauffmann et al. 1999). Here we use only the GIF simulation with $\Omega_0 = 0.3$ and $\Lambda_0 = 0.7$, for which the box length was $141.2h^{-1}$ Mpc (comoving) and the particle mass was $1.4 \times 10^{10}h^{-1}$ Mpc.

Galaxy, halo, and particle files are all easily downloaded from the GIF project website, <http://www.mpa-garching.mpg.de/GIF>, for a wide range of redshifts. Here we make use of only the present-epoch ($z = 0$) data, and the specific galaxy catalog that provides magnitudes in the SDSS band passes. The SDSS magnitudes of the GIF galaxies were converted to equivalent b_J magnitudes using the transformation given by equation (1) and, consistent with our adopted cosmological parameters, the absolute b_J magnitudes of the GIF galaxies were determined using the luminosity function of Norberg et al. (2002):

$$M_{b_J}^* - 5 \log_{10} h = -19.66 \pm 0.07. \quad (3)$$

Hosts and satellites in the GIF simulation were selected by rotating the simulation randomly and projecting the galaxy distribution along the line of sight. In order to mimic the 2dFGRS data set more closely, and to test our prescription for accounting for the velocity errors in the 2dFGRS data, Gaussian-distributed errors with $\sigma_{cz} = 85$ km sec⁻¹ were added to the line of sight velocities of the GIF galaxies. Different velocity errors were assigned to each galaxy for each rotation of the simulation box. (The velocity errors will, of course, not only affect the measured velocity dispersion of the satellites, but they will also affect the ultimate selection of hosts and satellites from the galaxy catalog.) After the addition of the velocity errors, the host-satellite selection criteria which were applied to the 2dFGRS data were then applied to the GIF galaxies. For each rotation of the simulation, the number of hosts and satellites was similar to that of the 2dFGRS data: ~ 1200 hosts and ~ 4100 satellites on average. A total of 100 random rotations of the simulation box were performed, and the results shown in all figures correspond to the mean over these 100 rotations.

The distribution of host luminosities of the GIF galaxies is shown in the right panel of Fig. 1 where, as with the 2dFGRS hosts, we have restricted the sample to those hosts with $0.5 L_{b_J}^* \leq L \leq 5.5 L_{b_J}^*$. While the luminosity distribution is fairly similar for the 2dFGRS and GIF hosts, the GIF hosts are somewhat more luminous than the 2dFGRS hosts ($L_{\text{med}} = 2.3 L_{b_J}^*$ for the 2dFGRS hosts; $L_{\text{med}} = 2.7 L_{b_J}^*$ for the GIF hosts). The

right panel of Fig. 2 shows the distribution of the number of satellites per host in the GIF simulation and, like the 2dFGRS galaxies, the sample consists primarily of hosts that have only 1 or 2 satellites, although there are certainly a larger percentage of GIF hosts with 3 or more satellites. On the whole, however, the host and satellite samples in the 2dFGRS and the GIF simulation are quite well-matched.

3. Computation of $\sigma_v(r_p)$ and Correction for Velocity Errors

The velocity dispersion of the satellite galaxies was computed using the method championed by McKay et al. (2002) and Prada et al. (2003). The distribution of the observed velocity differences between the hosts and satellites, $P(|dv|)$, for satellites with projected radii $r_1 < r_p \leq r_2$ is modeled as the sum of a Gaussian distribution and a constant offset that accounts for the presence of interlopers in the satellite sample. For all of the host-satellite samples considered here, this method works well and yields typical values of χ^2 per degree of freedom in the range $0.7 \lesssim \chi^2/\nu \lesssim 1.0$.

Similar to the results of van den Bosch et al. (2004), our own study of the GIF simulation suggests that, indeed, the fraction of interlopers for host-satellite pairs with small values of $|dv|$ exceeds that for host-satellite pairs with large values of $|dv|$. However, the effect is significantly smaller in the GIF simulation than was reported by van den Bosch et al. (2004). In addition, like van den Bosch et al. (2004) we find that, for a given distribution of velocity differences, $P(|dv|)$, the inferred velocity dispersion is not terribly sensitive to the interloper fraction. In particular, for a given $P(|dv|)$, varying the interloper fraction from $f_i \sim 0.1$ to $f_i \sim 0.4$ results in a change in the value of σ_v obtained from a Gaussian-plus-offset fit that is substantially less than the formal error bars on σ_v . We therefore conclude that, to within our formal error bars, the Gaussian-plus-offset fit to $P(|dv|)$ is sufficient to determine reasonable estimates of σ_v .

Shown in Fig. 3 is the velocity dispersion of the satellites in the GIF simulation, measured as a function of projected radius from the host. The solid triangles show the results for a “raw” measurement of $\sigma_v(r_p)$ in which the velocity errors have been included in the determination of $P(|dv|)$. The open circles show the results for a measurement of $\sigma_v(r_p)$ in which no velocity errors were assigned to either the hosts or the satellites. As expected, the inclusion of velocity errors inflates the measured velocity dispersion of the satellites above what would be obtained in the absence of velocity errors. Naively, of course, one would expect the velocity errors to add in quadrature with the true velocity dispersion and, hence, in a given radial bin the velocity dispersion which would be observed in the presence of the errors should be:

$$\sigma_v^{\text{obs}} = \sqrt{(\sigma_v^{\text{true}})^2 + 2(\sigma_{cz})^2}, \quad (4)$$

where σ_{cz} is the typical error in the line of sight velocity for a single galaxy. However, since the hosts and satellites are selected in part on the basis of velocity differences, the velocity errors will also enter in to the very definition of the sample itself and, in principle, a naive correction of the velocity dispersion using the above relation might not be sufficient.

The solid squares in Fig. 3, however, show that the naive correction to the velocity dispersion is sufficient. That is, the solid squares show the results of applying equation (4) above to the solid triangles, where we can see a good agreement between the corrected velocity dispersion profile and the velocity dispersion profile that was computed in the absence of velocity errors. We will, therefore, use equation (4) to correct the measured velocity dispersions of the satellites in both the 2dFGRS and GIF data, where a value of $\sigma_{cz} = 85 \text{ km sec}^{-1}$ is adopted.

4. Results

4.1. Interloper Fraction

As discussed by Prada et al. (2003) and Brainerd & Specian (2003), the fraction of interlopers is a strong function of projected radius. This is due to a geometrical effect; since the volume being searched for satellites increases with projected radius from the host, the number of interlopers will necessarily increase with projected radius.

Shown in Fig. 4 is the interloper fraction for the 2dFGRS sample, as well as the interloper fraction obtained for the GIF samples in which errors were added to the line of sight velocities. Again, the interloper fraction is determined by the constant offset component that is included when modeling the observed distribution of velocity differences as a Gaussian plus an offset. As with the luminosity distribution of the hosts (Fig. 1) and the distribution of the number of satellites (Fig. 2), we can see that the 2dFGRS and GIF samples seem to be well-matched to each other and, hence, a direct comparison of the results from each would seem to be justified.

4.2. Velocity Dispersion Profile for Complete Sample

Shown in Fig. 5 is the radial dependence of the velocity dispersion of the satellites in the full 2dFGRS sample, as well as the velocity dispersion of satellites in the GIF simulation for which velocity errors were added. In both cases, the measured velocity dispersions have been corrected for the velocity errors using equation (4) above with $\sigma_{cz} = 85 \text{ km sec}^{-1}$ and the interloper fraction was allowed to vary with projected radius (i.e., Fig. 4). Clearly, there is a very good agreement between the velocity dispersion of satellite galaxies in the 2dFGRS and the predictions of a Λ -dominated CDM universe. The velocity dispersion decreases with radius, similar to the results of Prada et al. (2003) for the SDSS galaxies, and shows that, as anticipated, the apparent disagreement between Brainerd & Specian (2003) and Prada et al. (2003) over the radial dependence of σ_v is due to the substantially larger error bars in the Brainerd & Specian (2003) analysis.

A close examination of the velocity dispersion profiles on scales $\lesssim 300h^{-1} \text{ kpc}$ in Fig. 5 shows that $\sigma_v(r_p)$ for the satellites in the GIF simulation has a somewhat higher amplitude and a somewhat steeper slope than that for the 2dFGRS satellites. This is likely due to the fact that, while the host samples are similar in the two data sets, they are not identical. In particular, the median luminosity of GIF hosts is larger than that of the 2dFGRS hosts by $\sim 0.4 L_{b_j}^*$. Based on known scaling relations of the internal velocity dispersion (or circular velocity) with galaxy luminosity, we certainly anticipate that the velocity dispersion of satellites of intrinsically bright galaxies will be larger than that of satellites of intrinsically faint galaxies. We will revisit this in §4.4 below.

Given the overall good agreement between $\sigma_v(r_p)$ for the 2dFGRS and GIF galaxies, it is not unreasonable to extend our analysis further and to investigate the dependence of the satellite velocity dispersion profile on host spectral type and host luminosity. The signal-to-noise will necessarily be lower when we subdivide the samples but, based on the strength of the signal in Fig. 5, it should be possible to place some modest constraints on the differences between the dynamics of satellites of hosts with differing spectral types and differing luminosities.

4.3. Dependence of Velocity Dispersion Profile on Host Spectral Type

The distribution of host spectral types in the 2dFGRS host sample is shown in the left panel of Fig. 6, where the parameter η is defined in Madgwick et al. (2002). Approximately one third of the hosts have $\eta \leq -2.45$, one third of the hosts have $-2.45 < \eta < -1.1$, and one third of the hosts have $\eta \geq -1.1$. From Fig. 4 of Madgwick et al. (2002), the morphologies of

these host galaxies should be approximately E/S0 ($\eta \leq -2.45$), Sa ($-2.45 < \eta < -1.1$), and Sb/Scd ($\eta \geq -1.1$). The luminosity distributions of the hosts within these subsamples is similar, with median luminosities of $2.64 L_{b_J}^*$ ($\eta \leq -2.45$), $2.25 L_{b_J}^*$ ($-2.45 < \eta < -1.1$), and $2.11 L_{b_J}^*$ ($\eta \geq -1.1$). We also note that, although the 2dFGRS team has provided eyeball morphologies for some of the galaxies, these are restricted to only the brightest hosts in our sample ($b_J \lesssim 18$) and choosing to subdivide the sample based on η rather than eyeball morphology will allow for the largest possible subsamples of hosts. In addition, a cursory examination of a subset of the hosts that have 2dFGRS eyeball classifications of “spiral” shows that some of these objects have spectra that are inconsistent with spiral morphology (i.e., their spectra are strongly dominated by absorption lines) and, so, the reliability of the eyeball classification seems to be somewhat questionable.

As above, we compute the velocity dispersions of the satellites about the hosts, allowing for the fact that the interloper fraction will increase with projected radius. The results are shown in Fig. 7, where it is clear that the velocity dispersion profiles of the satellites of early-type hosts are significantly different from those of late-type hosts. That is, while in all three cases the velocity dispersion profiles are decreasing, $\sigma_v(r_p)$ has a much higher amplitude and steeper decline for the satellites of early-type hosts than it does for the satellites of late-type hosts. Although there is some difference in the median luminosities of hosts with different values of η , we will show below that they are not sufficiently different for the trends in $\sigma_v(r_p)$ in Fig. 7 to be caused primarily by the differences in host luminosity. In other words, the differences in the three panels of Fig. 7 are most strongly correlated the spectral type of the host, not its luminosity.

Differences in the velocity dispersion profiles for the halos of elliptical galaxies and spiral galaxies are, of course, expected at some level due to the fact that the ellipticals are very likely to be merger products. While we cannot compare the predictions of the GIF simulation directly to the results of the 2dFGRS on the basis of the spectral parameter, we can at least compare the results for GIF hosts of differing color. Shown in the right panel of Fig. 6, then, is the distribution of $(g' - r')$ colors for the hosts in the GIF simulation. The distribution is clearly bi-modal and, so, we investigate the velocity dispersion of the satellites of “blue” GIF hosts, $(g' - r') < 0.2$, and “red” GIF hosts, $(g' - r') > 0.2$. We also note that, although a bi-modality in the $(g' - r')$ colors of SDSS galaxies is well-established (e.g., Baldry et al. 2004; Hogg et al. 2004; Blanton et al. 2003; Kauffmann et al. 2003), the bi-modality seen in the right panel of Fig. 6 is much sharper than that shown by the SDSS galaxies, and the median value of $(g' - r')$ for the “blue” GIF hosts is much bluer than that of the SDSS galaxies. This is, of course, simply a reflection of the fact that while the GIF simulation yields some remarkable agreements with the known local galaxy populations, it is not perfect in its representation.

The results for the velocity dispersion profiles of the satellites of blue and red GIF hosts are shown in Fig. 8 and, at least qualitatively, they are in general agreement with the results for the 2dFGRS hosts. That is, $\sigma_v(r_p)$ for the satellites of the red GIF hosts has a much higher amplitude than that for the satellites of the blue GIF hosts. In addition, $\sigma(r_p)$ for the satellites of the red GIF hosts decreases more rapidly with projected radius than does $\sigma_v(r_p)$ for the blue GIF hosts. However, $\sigma_v(r_p)$ for the satellites of the red GIF hosts has a lower amplitude and a shallower slope than does $\sigma_v(r_p)$ for the satellites of the early-type 2dFGRS hosts (i.e., left panel of Fig. 7). This disagreement persists even if we restrict our analysis to the very reddest GIF hosts; i.e., we obtain the same velocity dispersion profile for GIF hosts with $(g' - r') > 0.45$ as we do for GIF hosts with $(g' - r') > 0.2$. Similar to the satellites of the red GIF hosts, $\sigma_v(r_p)$ for the satellites of the blue GIF hosts has a lower amplitude than $\sigma_v(r_p)$ for the late-type 2dFGRS hosts (i.e., middle and right panels of Fig. 7). In addition, the slope of $\sigma_v(r_p)$ for the satellites of the blue GIF hosts is consistent with zero, while $\sigma_v(r_p)$ decreases for the satellites of the late-type 2dFGRS hosts.

4.4. Dependence of Velocity Dispersion Profile on Host Luminosity

On the basis of the Tully–Fisher and Faber–Jackson relations, we expect the velocity dispersions of the satellite galaxies to be strongly correlated with the luminosities of the host galaxies. Shown in Fig. 9, then, are the velocity dispersion profiles for the satellites of four independent subsamples of the hosts, where the median host luminosity in the subsamples is $L_{b,J}^*$ (top left panel), $2 L_{b,J}^*$ (top right panel), $3 L_{b,J}^*$ (bottom right panel), and $4 L_{b,J}^*$ (bottom right panel). Solid squares show the results for satellites of the GIF hosts, and open circles with error bars show the results for satellites of the 2dFGRS hosts. Although the signal-to-noise is somewhat low for $\sigma_v(r_p)$ for the satellites of the 2dFGRS galaxies, overall there is excellent agreement between the results for the 2dFGRS galaxies and the GIF galaxies. In addition, close examination of Fig. 9 shows that as the median luminosity of the host increases, both the amplitude and the slope of $\sigma_v(r_p)$ increase. Given the good agreement between the 2dFGRS and GIF galaxies in each of the individual panels of Fig. 9, then, the small differences in $\sigma_v(r_p)$ that are seen on scales $\lesssim 300h^{-1}$ kpc in Fig. 5 are most likely due to the fact that the distribution of host luminosities is somewhat different in the GIF simulation than it is in the 2dFGRS.

Finally, in Fig. 10 we show the dependence of the velocity dispersion of the satellites as a function of host luminosity for small projected radii ($r_p \leq 84h^{-1}$ kpc; i.e., $r_p \leq 120$ kpc for our adopted value of H_0). The choice of this particular physical scale is motivated by making a direct comparison to the results of Prada et al. (2003), who computed σ_v for the satellites

of SDSS galaxies as a function of host absolute magnitude for projected radii $r_p \leq 120$ kpc. As with Fig. 9, we again see a very good agreement between the results for the satellites of the 2dFGRS galaxies and the GIF galaxies. The relationship between σ_v and host luminosity is well-fitted by a power law of index 0.45, where the error on the power law index is 0.10 for the 2dFGRS satellites. This is somewhat steeper than one would expect on the basis of the local B-band Tully–Fisher relation, $\sigma_v \propto L^{0.3}$ (Verheijen 2001), but is only discrepant at less than the 2σ level.

5. Discussion

Here we have investigated the radial dependence of the velocity dispersion of satellite galaxies about host galaxies in an observational sample (the 2dFGRS) and a theoretical sample (the Λ CDM GIF simulation). Hosts and satellites were selected from the observational and theoretical samples using identical criteria, and velocity errors which are comparable to the velocity errors in the observational sample were added to the line of sight velocities in the theoretical sample. Overall, there is a remarkable similarity between the observational and theoretical samples of hosts and satellites (e.g., similar number of hosts and satellites, similar host luminosity distribution, similar number of satellites per host, and a similar fraction of interlopers).

We have shown that a simple correction for the errors that were added to the line of sight velocities of the GIF galaxies successfully reproduces the velocity dispersion profile that is measured in the absence of these errors. Further, when we correct the measured velocity dispersion profile of the full sample of 2dFGRS satellites using the same simple correction, we find a very good agreement of $\sigma_v(r_p)$ for the 2dFGRS satellites and $\sigma_v(r_p)$ for the GIF satellites. Further, $\sigma_v(r_p)$ decreases with r_p and on the large physical scales investigated here, this decrease is consistent with the expectations of NFW halos.

We have investigated the dependence of $\sigma_v(r_p)$ on the host spectral type, η , in the 2dFGRS and find a clear difference between the velocity dispersion profiles of the satellites of early-type hosts and late-type hosts. Although all of the velocity dispersion profiles decrease with r_p , both the amplitude and the slope of $\sigma_v(r_p)$ for the satellites of early-type hosts are substantially larger than those for the satellites of late-type hosts. This general trend is also shown by the satellites of the GIF hosts, where both the slope and the amplitude of $\sigma_v(r_p)$ for the satellites of the red GIF hosts are larger than those for the satellites of the blue GIF hosts. The differences in $\sigma_v(r_p)$ for hosts of differing color are, however, much less marked in the simulation than they are in the 2dFGRS.

We have also investigated the dependence of $\sigma_v(r_p)$ on the host luminosity, and find good agreement between the satellites of the 2dFGRS galaxies and the GIF galaxies. In all cases, $\sigma_v(r_p)$ decreases with r_p and both the slope and the amplitude of $\sigma_v(r_p)$ increase with host luminosity. In addition, the small-scale ($r_p \leq 84h^{-1}$ kpc) velocity dispersion of the satellites scales identically with host luminosity in the 2dFGRS and GIF samples: $\sigma_v \propto L^{0.45}$.

A velocity dispersion profile that decreases at large projected radii is, of course, expected in CDM universes. In addition, based on the known scalings of internal velocity dispersion or circular velocity with the luminosity of the galaxy, we expect the amplitude of $\sigma_v(r_p)$ to increase with increasing host luminosity. Our results for $\sigma_v(r_p)$ as a function of host luminosity (i.e., Fig. 9) show precisely this trend, and are in good agreement with the results of Prada et al. (2003) for the velocity dispersion profiles of the satellites of SDSS galaxies. The most direct comparison between our results and those of Prada et al. (2003) is the upper right panel of Fig. 9 in this paper and Fig. 7 of Prada et al. (2003). In this case our hosts have $L_{\text{med}} = 2L_{b_j}^*$ and the hosts in Prada et al. (2003) have comparable luminosities ($-20.5 < M_B < -21.5$). Comparing these two figures, we find an excellent agreement of both the slope and the amplitude of $\sigma_v(r_p)$ in these independent analyses. Fig. 8 of Prada et al. (2003) shows $\sigma_v(r_p)$ for fainter SDSS hosts ($-19.5 < M_B < -20.5$), and shows a clear decrease in the amplitude compared to their results for brighter hosts. Unfortunately, the faintest luminosity subsample in our work (top left panel of Fig. 9 in this paper) is somewhat too bright to be compared directly to the faintest subsample in Prada et al. (2003). As result, although we do see a clear decrease in the amplitude of $\sigma_v(r_p)$ in going from the top right panel to the top left panel of our Fig. 9, the decrease is not as substantial as seen when comparing Figs. 7 and 8 of Prada et al. (2003). Finally, the slope of $\sigma_v(r_p)$ in the Prada et al. (2003) analysis does not appear to increase as a function of host luminosity; however, the increase in the slope of $\sigma_v(r)$ with host luminosity in our Fig. 9 is sufficiently gradual that it likely would not have been obvious for the range of host luminosities shown in Figs. 7 and 8 of Prada et al. (2003).

The dependence of the small-scale ($r_p \leq 84h^{-1}$ kpc) satellite velocity dispersion with host luminosity is, however, only marginally consistent between this work and that of Prada et al. (2003), who found $\sigma_v \propto L^{0.3}$ for the same physical scale. The explanation for this is unclear, but given the wide range of published constraints on halo velocity dispersions from both dynamical and weak lensing studies, this apparent discrepancy is perhaps not unexpected. Based on satellite dynamics, the constraints on the value of the index of the Tully–Fisher relation range from approximately zero (i.e., Zaritsky et al. 1997) to 1 (Brainerd & Specian 2003), with rather large error bars. Complicating matters further, these dynamical constraints come from different physical scales and the only results that can truly be compared directly are those of this work and Prada et al. (2003). Similarly, weak lensing

constraints on the value of the index of the Tully–Fisher index range from 0.3 to 1.7 (e.g., Hudson et al. 1998; McKay et al. 2001; Smith et al. 2001; Kleinheinrich et al. 2003, 2004). The weak lensing measurement that claims the most accurate value, $0.30_{-0.12}^{+0.16}$ (Kleinheinrich et al. 2004), is in modest agreement with our value but, again, the weak lensing measurement is made over a somewhat larger physical scale ($\lesssim 150h^{-1}$ kpc) and, moreover, was determined for lens galaxies with much higher redshifts than our host galaxies.

Finally, this work and Brainerd & Specian (2003) are, so far, the only investigations of satellite dynamics to be performed as a function of the host spectral type or morphology. Brainerd & Specian (2003) used the eyeball morphologies provided by the 2dFGRS team for the 100K data release to divide their sample into 159 hosts with elliptical or S0 morphologies and 243 hosts with spiral morphologies. Unlike this work, Brainerd & Specian (2003) found that $\sigma_v(r_p)$ was independent of r_p for the satellites of both the early– and late–type hosts; however, the error bars in Brainerd & Specian (2003) were larger due to the relatively small sample sizes and, so, a decrease in $\sigma_v(r_p)$ at the level that we see here would not have been detected in their data. In addition, our recent examination of the spectra of 2dFGRS hosts with eyeball classifications of “spiral” suggest that at least some have been misclassified (c.f. §4.3 above) and, so, a detailed comparison of this investigation and that of Brainerd & Specian (2003) is somewhat questionable.

However, our observed general trend for the velocity dispersion of the satellites of early–type hosts to be greater than that of the satellites of late–type hosts is in agreement with recent weak lensing constraints on σ_v for the halos of galaxies with differing morphology. In particular, Kleinheinrich et al. (2003) find that, averaged over projected radii of $20h^{-1}$ kpc $\leq r_p \leq 150h^{-1}$ kpc, the velocity dispersion of L^* early–type lenses is 198_{-42}^{+32} km sec $^{-1}$, while for L^* late–type lenses it is 146_{-38}^{+32} km sec $^{-1}$. From Fig. 7, the velocity dispersion of the satellites in the 2dFGRS averaged over a similar scale is ~ 290 km sec $^{-1}$ for hosts with $\eta \leq -2.45$, ~ 230 km sec $^{-1}$ for hosts with $-2.45 < \eta < -1.1$, and ~ 160 km sec $^{-1}$ for hosts with $\eta \geq -1.1$. The median luminosities of the 2dFGRS hosts are, of course, brighter than $L_{b_j}^*$, so we would expect the mean velocity dispersions of the satellites to exceed the values found by Kleinheinrich et al. (2003). Based on the scaling of σ_v with host luminosity that we found in Fig. 10, we would expect the velocity dispersion of early–type lenses with $L = 2L^*$ in the Kleinheinrich et al. (2003) sample to be of order 300 km sec $^{-1}$ and the velocity dispersion of late–type lenses with $L = 2L^*$ to be of order 200 km sec $^{-1}$. Both of these are in quite reasonable agreement with our results for the 2dFGRS satellites as a function of host spectral type, where the late–type hosts are expected to be those with $\eta > -2.45$.

We conclude that the dynamics of the satellite galaxies in the 2dFGRS are in good agreement with the expectations for satellite galaxies in a Λ CDM universe, and that the

available samples of hosts and satellites in current redshift surveys are now becoming sufficiently large that they can be used to study the dark matter halos of the hosts. Given the potential complications in the interpretation of galaxy–galaxy lensing data (e.g., multiple weak deflections caused by foreground galaxies, as well as galaxy lenses being embedded within groups and clusters), the use of the dynamics of satellites to study the dark matter halos of large galaxies is likely to emerge as a useful technique that is entirely complementary to galaxy–galaxy lensing.

It is a pleasure to thank the members of the 2dFRGS team and the GIF project for not only making their data publicly–available, but also for making their data products superbly easy to obtain and use. Support under NSF contract AST–00984572 is also gratefully acknowledged.

REFERENCES

- Baldry, I. K., Glazebrook, K., Brinkmann, J., Ivezić, Z., Lupton, R. H., Nichol, R. C. & Szalay, A. S. 2004, *ApJ*, 600, 681
- Blanton, M. R., Hogg, D. W., Bahcall, N. A., Baldry, I. K., Brinkmann, J., Csabai, I., Eisenstein, D., Fukugita, M., Gunn, J. E., et al. 2003, *ApJ*, 594, 186
- Brainerd, T. G. 2003, in proceedings of “Hubble’s Science Legacy: Future Optical–UV Astronomy from Space”, ASP Conf. Series vol. 291, eds. Sembach, K. R., Blades, J. C., Illingworth, G. D. & Kennicutt, R. C., 347
- Brainerd, T. G. 2004, to be published in the proceedings of IAU Symposium 225, “The Impact of Gravitational Lensing on Cosmology”, eds. Y. Mellier & G. Meylan, astro–ph/0409374
- Brainerd, T. G., Blandford, R. D. & Smail, I. 1996, *ApJ*, 466, 623 (BBS)
- Brainerd, T. G. & Specian, M. A. 2003, *ApJ*, 593, L7
- Colless, M., Dalton, G., Maddox, S., Sutherland, W., Norberg, P., Cole, S., Bland–Hawthorn, J., et al. 2001, *MNRAS*, 328, 1039
- Colless, M., Peterson, B. A., Jackson, C., Peacock, J. A., Cole, S., Norberg, P., Baldry, I. K. et al. 2003 (astro–ph/0306581)

- Conroy, C., Newman, J. A., Davis, M., Coil, A. L., Yan, R., Cooper, M. C., Gerke, B. F., Faber, S. M. & Koo, D. 2004 (astro-ph/0409305)
- Fischer, P., McKay, T. A., Sheldon, E., Connolly, A., Stebbins, A., Frieman, J. A., Jain, B., et al. 2001, *AJ*, 120, 1198
- Griffiths, R. E., Casertano, S., Im, M. & Ratnatunga, K. 1996, *MNRAS*, 282, 1159
- Guzik, J. & Seljak, U. 2002, *MNRAS*, 335, 311
- Hoekstra, H., Franx, M., Kuijken, K., Carlberg, R. G. & Yee, H. K. C. 2003, *MNRAS*, 340, 609
- Hoekstra, H., Yee, H. K. C. & Gladders, M. D. 2004, *ApJ*, 606, 67
- Hogg, D. W., Blanton, M. R., Brinchmann, J., Eisenstein, D. J., Schlegel, D. J., Gunn, J. E., McKay, T. A., Bahcall, N. A., Brinkmann, J. & Meiksin, A. 2004, *ApJ*, 601, L29
- Maddox, S. J., Efstathiou, G., Sutherland, W. J. & Loveday, J. 1990a, *MNRAS*, 243, 692
- Maddox, S. J., Efstathiou, G., Sutherland, W. J. & Loveday, J. 1990b, *MNRAS*, 246, 433
- Madgwick, D. S., Lahav, O., Baldry, I. K., Baugh, C. M., Bland–Hawthorn, J., Bridges, T., Cannon, R., Cole, S., Colless, M., et al. 2002, *MNRAS*, 333, 133
- Norberg, P., Cole, S., Baugh, C. M., Frenk, C. S., Baldry, I., Bland–Hawthorn, J., Bridges, T., Cannon, R., Colless, M., et al. 2002, *MNRAS*, 336, 907
- Navarro, J.F., Frenk, C.S. & White, S.D.M. 1995, *MNRAS*, 275, 720
- Navarro, J.F., Frenk, C.S. & White, S.D.M. 1996, *ApJ*, 462, 563
- Navarro, J.F., Frenk, C.S. & White, S.D.M. 1997, *ApJ*, 490, 493
- Kauffmann, G., Heckman, T. M., White, S. D. M., Charlot, S., Tremonti, C., Brinchmann, J., Bruzual, G., Peng, E. W., Seibert, M., et al. *MNRAS*, 341, 33
- Kauffmann, G., Colberg, J. M., Diaferio, A. & White, S. D. M. 1999, *MNRAS*, 303, 188
- Kleinheinrich, M., Schneider, P., Erben, T., Schirmer, M., Rix, H.–W. & Meisenheimer, K. 2003, to be published in the proceedings of “Gravitational Lensing: A Unique Tool for Cosmology” (astro-ph/0304208)

- Kleinheinrich, M., Rix, H.–W., Schneider, P., Erben, T., Meisenheimer, K., Wolf, C. & Schirmer, M. 2004, to be published in the proceedings of IAU Symposium 225, “The Impact of Gravitational Lensing on Cosmology”, eds. Y. Mellier & G. Meylan (astro-ph/0409320)
- McKay, T. A., Sheldon, E. S., Racusin, J., Fischer, P., Seljak, U., Stebbins, A., Johnston, D., et al. 2001 (astro-ph/0108013)
- McKay, T. A., Sheldon, E. S., Johnston, D., Grebel, E. K., Prada, F., Rix, H.–W., Bahcall, N. A., Brinkmann, J., et al. 2002, *ApJ*, 571, 85
- Prada, F., Vitvitska, M., Klypin, A., Holtzman, J. A., Schelgel, D. J., Grebel, E. K., Rix, H.–W., Brinkmann, J., McKay, T. A. & Csabai, I. 2003, *ApJ*, 598, 260
- Smith, D. R., Bernstein, G. M., Fischer, P. & Jarvis, M. 2001, *ApJ*, 551, 643
- Wilson, G., Kaiser, N., Luppino, G. A. & Cowie, L. L. 2001, *ApJ*, 555, 572
- van den Bosch, F. C., Norberg P., Mo, H. J. & Yang, X. 2004 (astro-ph/0404033)
- Verheijen, M. A. W. 2001, *ApJ*, 563, 694
- York, D. G., Adelman, J., Anderson, J. E., Anderson, S. F., Annis, J., Bahcall, N. A., Bakken, J. A., Barkhouser, R., et al. 2000, *AJ*, 120, 1579
- Zaritsky, D. & White, S. D. M. 1994, *ApJ*, 435, 599
- Zaritsky, D., Smith, R., Frenk, C. & White, S. D. M., 1997, *ApJ*, 478, 39

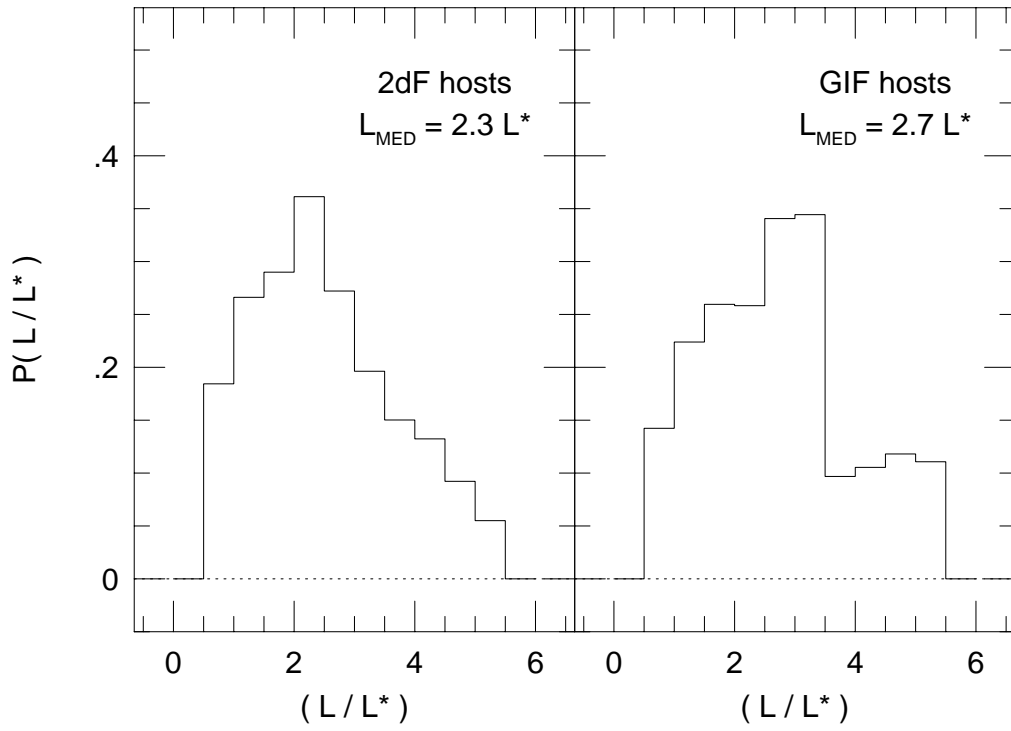


Fig. 1.— Left panel: Probability distribution of host galaxy luminosities in the 2dFGRS. The sample has been restricted to hosts with luminosities in the range $0.5 L_{b,j}^* \leq L_{\text{host}} \leq 5.5 L_{b,j}^*$. Right panel: Same as left panel, but for host galaxies in the GIF simulation.

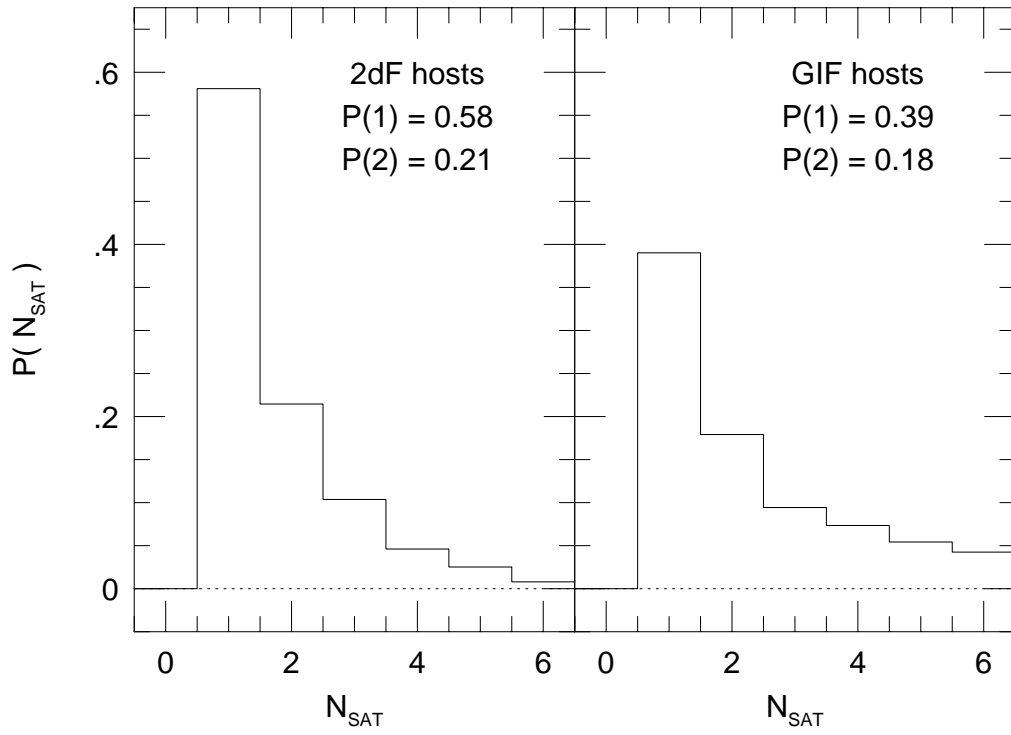


Fig. 2.— Left panel: Probability distribution of the number of satellite galaxies associated with host galaxies in the 2dFGRS. Here, by definition, each host galaxy has at least one satellite. Right panel: Same as left panel, but for host galaxies in the GIF simulation.

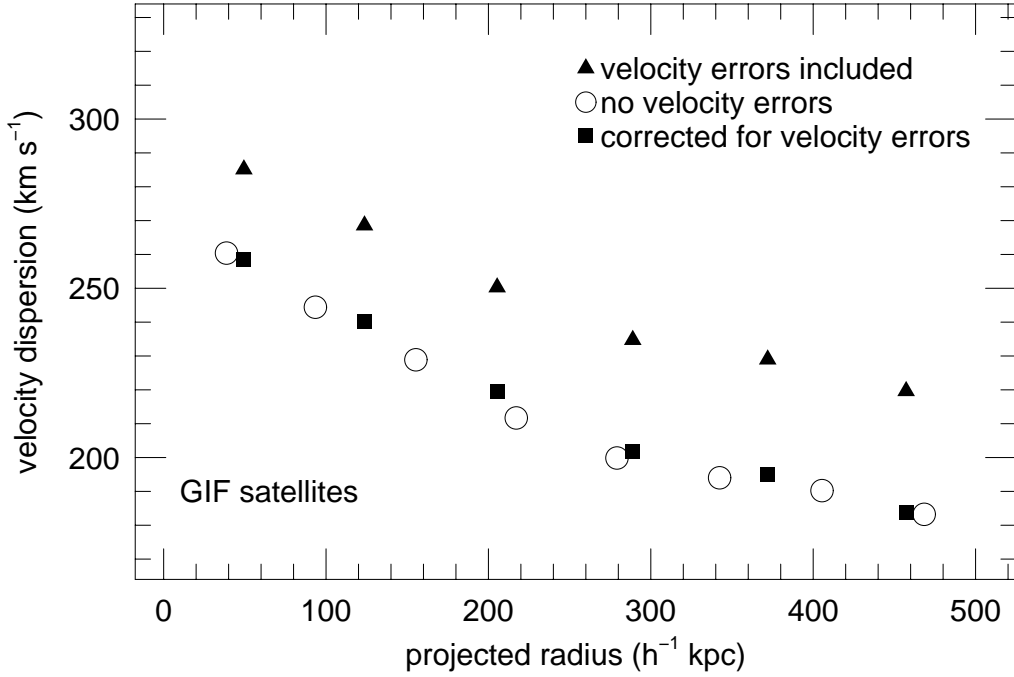


Fig. 3.— Velocity dispersion profile, $\sigma_v(r_p)$, for satellite galaxies in the GIF simulation. Here the interloper fraction has been allowed to vary with projected radius. Solid triangles show the raw values $\sigma_v(r_p)$ that are obtained when errors that are comparable to the errors in the line of sight velocities of the 2dFGRS galaxies are added to the line of sight velocities of the GIF galaxies. Open circles show $\sigma_v(r_p)$ that is obtained when no errors are added to the velocities of the GIF galaxies. Solid squares show $\sigma_v(r_p)$ that is obtained after correcting the solid triangles for the velocity errors using equation (4).

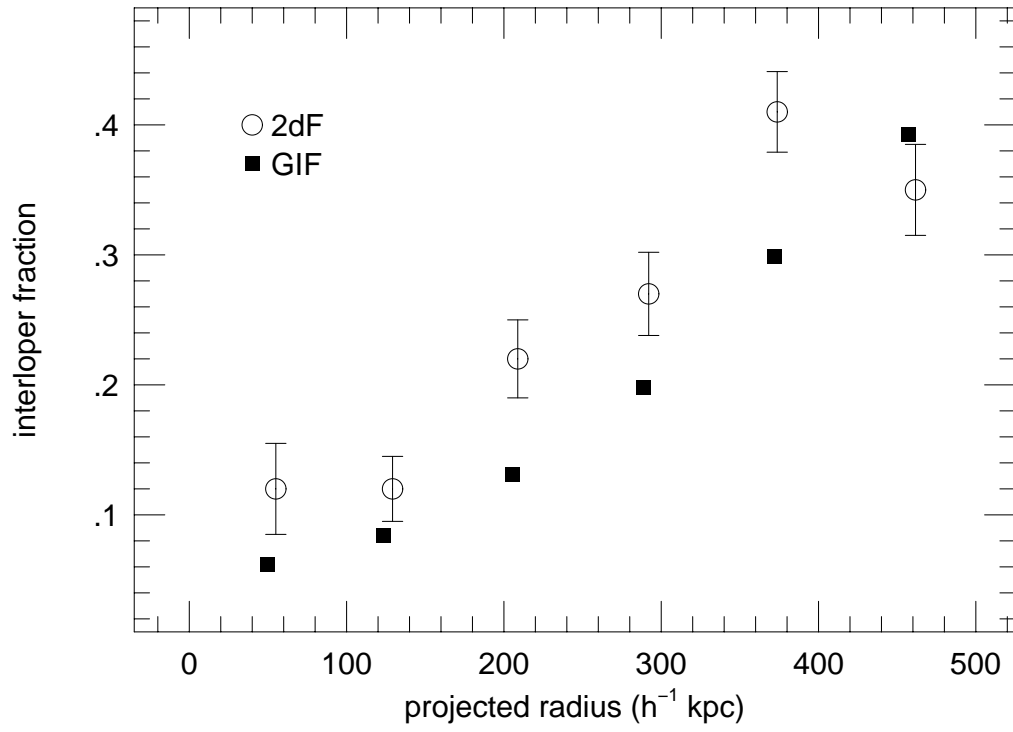


Fig. 4.— Interloper fraction as a function of radius in the 2dFGRS (open circles) and the GIF simulation (solid squares).

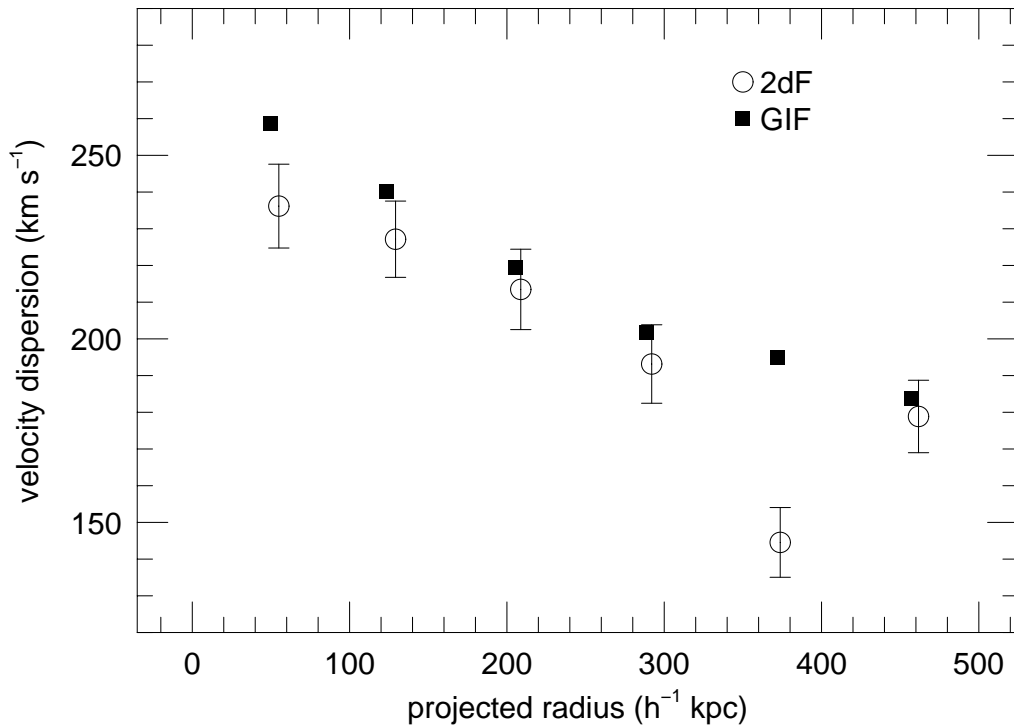


Fig. 5.— Velocity dispersion profiles for satellite galaxies in the 2dFGRS (open circles) and the GIF simulation (solid squares). Values of $\sigma_v(r_p)$ have been corrected for errors in the line of sight velocity using equation (4). On scales $\lesssim 300h^{-1}$ kpc, the slight difference between $\sigma_v(r_p)$ for the 2dFGRS satellites and $\sigma_v(r_p)$ for the GIF satellites is likely due to the difference in median luminosities of the 2dFGRS and GIF hosts (see §4.4 and Fig. 9).

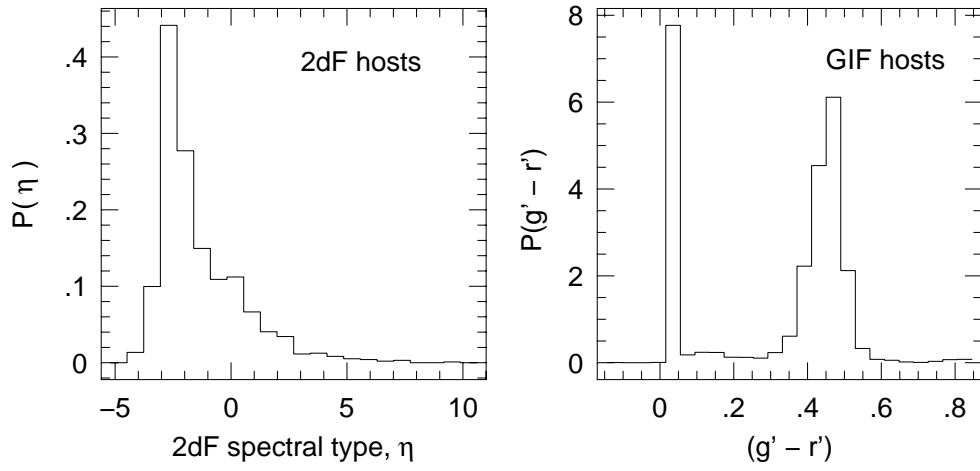


Fig. 6.— Left Panel: Probability distribution of host spectral type in the 2dFGRS. Right panel: Probability distribution of host $(g' - r')$ color in the GIF simulation.

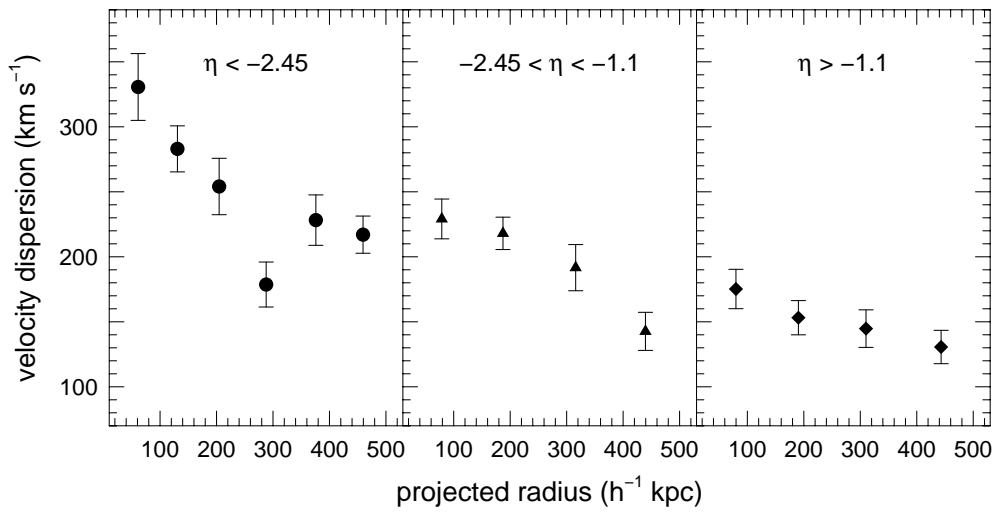


Fig. 7.— Dependence of 2dFGRS satellite velocity dispersion profiles on the spectral type of the host, η . Based on Fig. 4 of Madgwick et al. (2002), the morphology of the hosts is expected to be roughly E/S0 in the left panel, Sa in the middle panel, and Sb/Scd in the right panel. Values of $\sigma_v(r_p)$ have been corrected for errors in the line of sight velocity using equation (4).

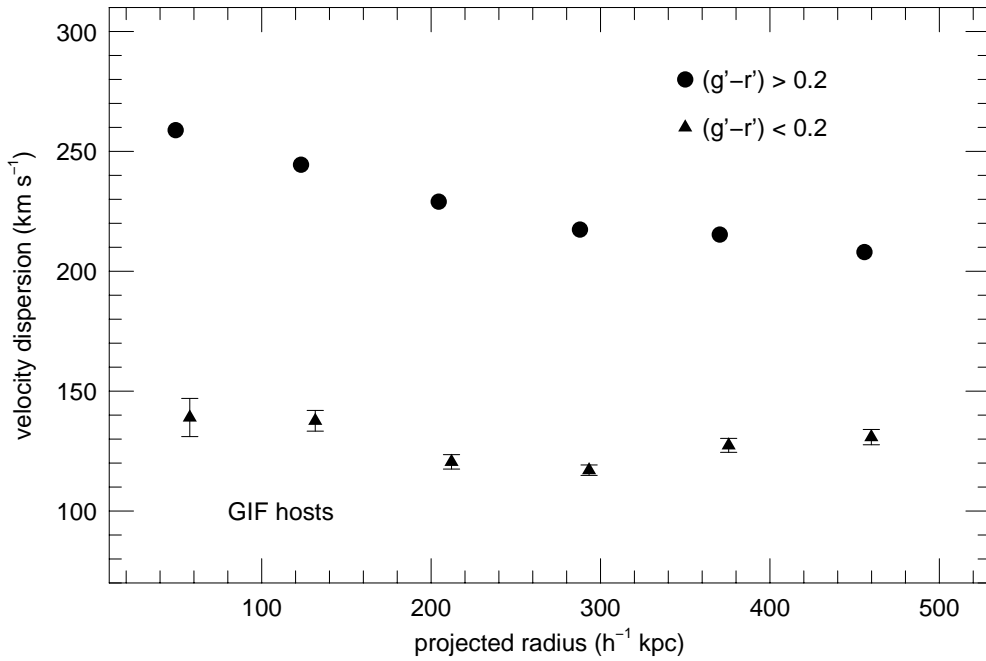


Fig. 8.— Dependence of GIF satellite velocity dispersion profiles on the $(g' - r')$ color of the host. Values of $\sigma_v(r_p)$ have been corrected for errors in the line of sight velocity using equation (4).

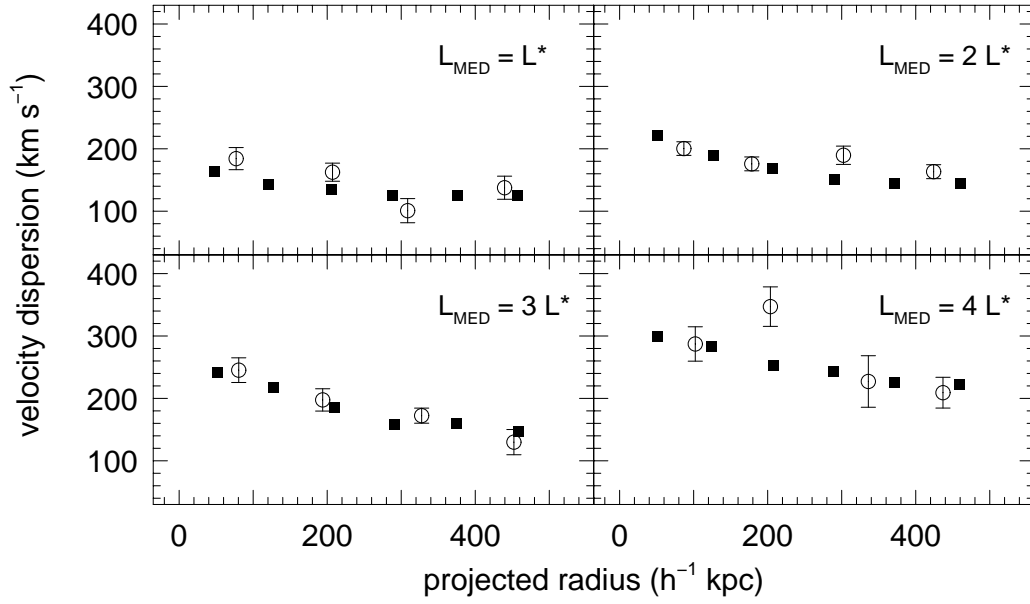


Fig. 9.— Dependence of satellite velocity dispersion profiles on the luminosity of the host (open circles: 2dFGRS; solid squares: GIF simulation). Values of $\sigma_v(r_p)$ have been corrected for errors in the line of sight velocity using equation (4).

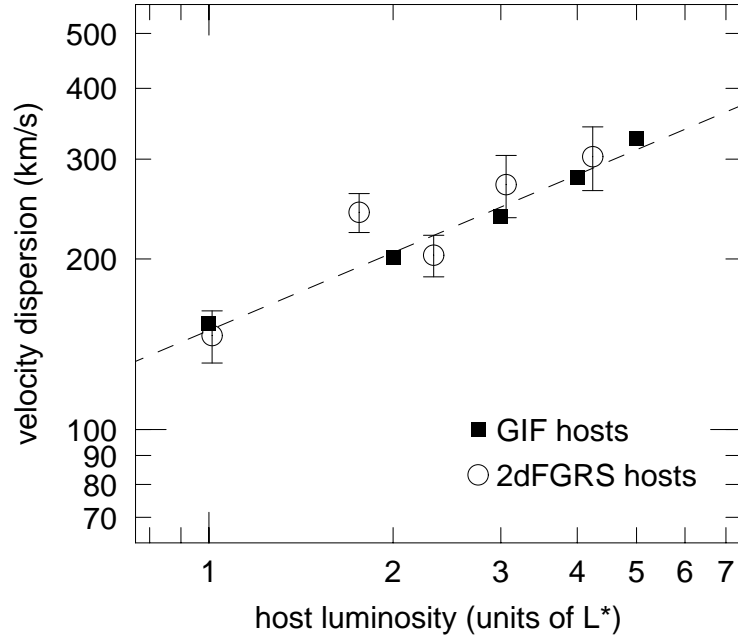


Fig. 10.— Dependence of satellite velocity dispersion on host luminosity for satellites with projected radii $r_p \leq 120$ kpc (i.e., $r_p \leq 84h^{-1}$ kpc). Open circles show results for the 2dFGRS galaxies; solid squares show results for the GIF galaxies. Dashed line shows $\sigma_v \propto L^{0.45}$, which is the best-fit to both the 2dFGRS galaxies and the GIF galaxies. Values of σ_v have been corrected for errors in the line of sight velocity using equation (4).